IEEE Access
Multidisciplinary | Rapid Review | Open Access Journal

Received November 3, 2018, accepted December 27, 2018, date of publication January 29, 2019, date of current version February 14, 2019.

Digital Object Identifier 10.1109/ACCESS.2019.2895919

Random Drift Modeling and Compensation for MEMS-Based Gyroscopes and Its Application in Handwriting Trajectory Reconstruction

YU-LIANG HSU[1], (Member, IEEE), AND JEEN-SHING WANG[2], (Member, IEEE)
[1]Department of Automatic Control Engineering, Feng Chia University, Taichung 40724, Taiwan
[2]Department of Electrical Engineering, National Cheng Kung University, Tainan 701, Taiwan

Corresponding author: Yu-Liang Hsu (hsuyl@fcu.edu.tw)

This work was supported by the Ministry of Science and Technology of the Republic of China, Taiwan, under Grants MOST 106-2221-E-035-004, MOST 107-2221-E-035-080, and MOST 106-3011-E-006-002.

ABSTRACT Microelectromechanical system (MEMS)-based gyroscopes have been widely applied to various inertial-sensing-based human–computer interaction (HCI) devices. However, the random drift of MEMS-based gyroscopes limits their applications. Hence, studies pay attention to develop various models to model and compensate the random drift for improving the performance of the MEMS-based gyroscopes. This paper presents a self-constructing Wiener-type recurrent neural network (SCWRNN) with its false nearest-neighbors-based self-constructing strategy and recursive recurrent learning algorithm to model the random drift of the MEMS-based gyroscopes and then compensate them from the calibrated gyroscope measurement. Subsequently, the proposed random drift modeling and compensation algorithm is integrated into the handwriting trajectory reconstruction algorithm of the inertial-sensing-based HCI device, called IMUPEN, for accurately obtaining the reconstructed handwriting trajectory. Users can hold the IMUPEN, which is composed of an accelerometer, two gyroscopes, a microcontroller, and an RF wireless transmission module, to write numerals at normal speed. The accelerations and angular velocities measured by the accelerometer and gyroscopes are transmitted to a personal computer through the RF module for further reconstructing the handwriting trajectory via the handwriting trajectory reconstruction algorithm. In addition, we have developed the SCWRNN-based random drift modeling and compensation algorithm to eliminate the cumulative errors caused by the random drift of the MEMS-based gyroscopes for further increasing the accuracy of handwriting trajectory reconstruction. Our experimental results have successfully validated the effectiveness of the proposed random drift modeling and compensation algorithm and its application in handwriting trajectory reconstruction.

INDEX TERMS Random drift modeling, MEMS-based gyroscope, recurrent neural network, handwriting trajectory reconstruction.

I. INTRODUCTION

In recent year, microelectromechanical system (MEMS)-based inertial sensors have gained great attention for their multiple field applications, such as activity recognition, sport science, medical rehabilitation, gait analysis, health care, inertial navigation, and robot teleoperation [1]–[10]. In addition, inertial-sensing-based human-computer interaction (HCI) methods have been widely developed to create new types of HCI remote control devices via activity recognition [11], gesture recognition [12], handwriting recognition [13], and motion tracking [14], etc.

Among various inertial-sensing-based HCI devices, pen-type HCI devices are embedded with accelerometers and gyroscopes for providing intuitive expressions, which can reconstruct handwriting trajectories without the limitations of writing range or dimensions by using the accelerations and angular velocities generated by handwriting movements [13]. A handwriting trajectory reconstruction depends on the integration process of the accelerations and angular

The associate editor coordinating the review of this manuscript and approving it for publication was Gerhard P. Hancke.

velocities measured by accelerometers and gyroscopes during executing handwriting movements. Subsequently, orientation angles can also be obtained through the single integral of angular velocities, which are used to form a transformation matrix for projecting the accelerations from the body coordinate to the reference coordinate. Then, the accelerations in the reference coordinate can be used to obtain the handwriting velocities and positions (trajectories) through the single integral and double integral processes, respectively. However, the accuracy of the handwriting trajectories usually contains the effects of errors of the inertial sensors. In practice, the accelerometer error introduces a second-order error in handwriting trajectory after double integral. In the meanwhile, the error of the gyroscope may lead to a first-order error in the orientation angle after single integral and a third-order error in handwriting trajectory, respectively [15]. Obviously, the accuracy of the handwriting trajectories of the pen-type inertial-sensing-based HCI devices is seriously affected by the performance of the gyroscope errors and quickly degrades over time. Therefore, to estimate and compensate the errors of the MEMS-based gyroscope is an important procedure for enhancing the performance of the handwriting trajectories of the pen-type HCI devices embedded with the MEMS-based inertial sensors.

In general, the errors of the inertial sensors include deterministic and stochastic errors [16], [17]. The deterministic errors contain scale factors and biases, which can be removed from the raw measurements in the calibration procedure. The stochastic errors called bias drift are random in nature and correlated over time, which can be modeled as a stochastic process for extenuating their deleterious effect on the accuracy of handwriting trajectory reconstruction. Currently, the common approach for modeling and compensating the random drift of the MEMS-based gyroscopes is time series analysis [17]–[19]. To name a few, Noureldin *et al.* [18] utilized a second-order autoregressive (AR) model to estimate the inertial sensors' drift error by using the stationary measurements of the inertial sensors. Zhang and Fang [19] identified the gyroscope drift by utilizing an autoregressive moving average (ARMA) model with the gyroscope measurements within 2 minutes firstly. Then, the performance of the MEMS-based gyroscope was improved via a Kalman filter which was applied to compensate the error. Alternatively, the artificial intelligence-based methods utilizing neural networks (NNs) have been developed for modeling the MEMS-based inertial sensor error and are found to have better performance than other common time series analysis techniques [16], [20]–[23]. Hao and Tian [20] utilized a grey radial basis network (GRBF) for estimating the MEMS-based gyroscope drift. Compared with AR models, the GRBF has better identification performance, but it needs more computational time. Xing *et al.* [22] applied a least squares support vector machine (LSSVM) to model and compensate the random drift of the MEMS-based gyroscope, which was optimized by the chaotic particle swarm optimization. Shen *et al.* [23] selected the temperature, temperature variation rate, and coupling term to be as the inputs for the genetic-Elman neural network which was utilized to model the temperature drift of the MEMS-based gyroscope.

In our literature review, we found that most existing artificial intelligence-based methods for modeling stochastic errors (random drift) are feedforward neural networks (FNNs). However, recurrent neural networks (RNNs) which provide feedback connections in addition to feedforward connections, have greater robustness for dealing with time series signals. In addition, neurons in hidden layers of NNs are determined based on expert experience and knowledge, which leads to computational complex and poor modeling accuracy. This paper targets to purpose a self-constructing Wiener-type RNN (SCWRNN) with its false nearest neighbors-based self-constructing strategy and recursive recurrent learning algorithm to model and compensate random drift of MEMS-based gyroscopes embedded in a pen-type inertial-sensing-based HCI device for improving the performance of handwriting trajectories. The proposed pen-type inertial-sensing-based HCI device called IMUPEN comprises an accelerometer, two gyroscopes, a microcontroller, and an RF wireless transmission module [13]. Users can hold this IMUPEN to write numerals at their preferred speed without any space limitations. Subsequently, the handwriting motion signal measured by the accelerometer and gyroscopes are submitted to a personal computer (PC) for further signal processing via the RF wireless module. Then, the handwriting trajectory reconstruction algorithm proposed in our earlier work [13] is adopted in this paper to reconstruct handwriting numeral trajectories. In order to model and compensate the random drift of the MEMS-based gyroscopes, we integrate the proposed random drift modeling and compensation algorithm into the handwriting trajectory reconstruction algorithm for acquiring more accurate handwriting trajectories. The contribution of this paper is to develop a SCWRNN with its false nearest neighbors-based self-constructing strategy and recursive recurrent learning algorithm to model the stochastic time series errors (random drift) of the MEMS-based gyroscopes and then compensate them from the calibrated gyroscope measurement by using the proposed random drift modeling and compensation algorithm for obtaining more accurate handwriting trajectories.

The remainder of this paper is organized as follows. The SCWRNN is introduced in detail In Section II. In Section III, we present the proposed random drift modeling and compensation algorithm. The experimental setup and results of random drift modeling and compensation of MEMS-based gyroscopes and handwriting trajectory reconstruction applications are provided in Section IV. Finally, conclusions are given in the Section V.

II. SELF-CONSTRUCTING WIENER-TYPE RECURRENT NEURAL NETWORK

A. WIENER-TYPE RECURRENT NEURAL NETWORK

The proposed self-constructing Wiener-type recurrent neural network (SCWRNN) shown in Fig. 1(a) is composed of an

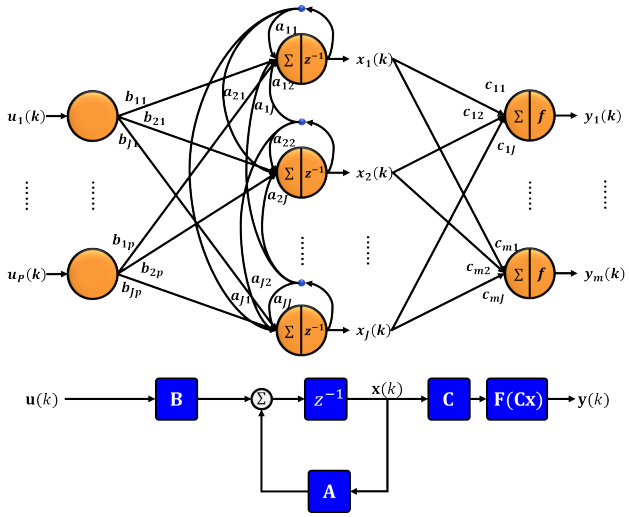

FIGURE 1. (a) The topology of the proposed SCWRNN. (b) The block diagram of the proposed SCWRNN.

input layer, a hidden layer, and an output layer. The input layer transmits the input values to the network and does not execute any operators. The hidden layer integrates the current input values from the input layer and the state history stored in the memories of the neurons in the hidden layer to infer the current states of the network. Finally, the state variables are transformed into the output space through a nonlinear mapping in the output layer. The $u_i^{(j)}(k), f_i^{(j)}(k)$, and $o_i^{(j)}(k)$ are represented as the input value, input function, and output of the activation function of the ith neuron in the jth layer at time k, respectively.

1) INPUT LAYER

The input neurons convey the input values to the hidden neurons directly. Therefore, the functions of the ith neurons in the first layer are represented as

$$f_i^{(1)}(k) = u_i^{(1)}(k), \tag{1}$$
$$o_i^{(1)}(k) = f_i^{(1)}(k). \tag{2}$$

2) HIDDEN LAYER

The functions of the jth neuron in the second layer can be defined as

$$f_j^{(2)}(k+1) = \sum_{i=1}^{J} a_{ji} x_i(k) + \sum_{h=1}^{P} b_{jh} u_h^{(1)}(k), \tag{3}$$
$$o_j^{(2)}(k) \triangleq x_j(k) = f_j^{(2)}(k), \tag{4}$$

where $x_j(k)$ is the state variables of the state space representation.

3) OUTPUT LAYER

The output neurons utilize hyperbolic tangent sigmoid functions to realize a nonlinear transformation from the state variables to the network output values. The functions of the neurons in the last layer are defined as

$$f_j^{(3)}(k) = \sum_{i=1}^{J} c_{ji} x_i(k), \tag{5}$$
$$y_j(k) = o_j^{(3)}(k) = \frac{\exp(f_j^{(3)}(k)) - \exp(-f_j^{(3)}(k))}{\exp(f_j^{(3)}(k)) + \exp(-f_j^{(3)}(k))}. \tag{6}$$

The total number of network parameters can be calculated by $N_p = J \times (J + p + m)$. Based on the proposed SCWRNN, we have developed a false nearest neighbors-based self-constructing strategy for determining the number of the hidden neurons using input-output data and a recursive recurrent learning algorithm for online tuning SCWRNN's parameters. Additionally, the SCWRNN can also be expressed by the following state space representation:

$$\mathbf{x}(k+1) = \mathbf{A}\mathbf{x}(k) + \mathbf{B}\mathbf{u}(k),$$
$$\mathbf{y}(k) = \mathbf{F}(\mathbf{C}\mathbf{x}(k)), \tag{7}$$

where $\mathbf{u} = [u_1, \ldots, u_p]^T$ is the input vector, $\mathbf{x} = [x_1, \ldots, x_J]^T$ is the state vector, $\mathbf{y} = [y_1, \ldots, y_m]^T$ is the output vector, $\mathbf{F} = [f_1, \ldots, f_m]^T$ is the nonlinear function vector, and p, J, and m are the total number of neurons of the input layer, hidden layer, and output layer, respectively. $\mathbf{A} \in \mathbb{R}^{J \times J}$ represents the weights of the self-feedback connections. $\mathbf{B} \in \mathbb{R}^{J \times p}$ is the link weights between the input layer and the hidden layer. $\mathbf{C} \in \mathbb{R}^{m \times J}$ represents the link weights between the hidden layer and the output layer. The block diagram of the proposed SCWRNN is shown as Fig. 1(b).

B. FALSE NEAREST NEIGHBORS-BASED SELF-CONSTRUCTING STRATEGY

Since the random drift of the MEMS-based gyroscope is a chaotic time series, we adopt the false nearest neighbors to estimate system order (number of state variables or hidden neurons) of the SCWRNN. The false nearest neighbors algorithm is widely used to determine the minimum embedding dimension of the chaotic systems by using input-output measurements [24], [25]. For a single-input-single-output (SISO) system, we assume that the current system output can be modeled by the history of input and output measurements.

$$\begin{aligned} y(k) &= f\left(\boldsymbol{\chi}_{(J,l)}(k)\right) \\ &= f([y(k-1), \ldots, y(k-J), u(k-1), \\ &\quad \ldots, u(k-l)]), \end{aligned} \tag{8}$$

where $y(k)$ and $u(k)$ represent the system output and input, respectively, $f(k)$ is the model of the system output, $\chi(k)$ denotes the corresponding regressor, J and l are the numbers of time-delayed observations for the system output and input in the regression vector, respectively. In the proposed SCWRNN, the value of J is the number of state variables or hidden neurons. Different numbers of the time-delayed terms are utilized in the regression vectors to calculate the percentage of regression vectors with false nearest neighbors for determining the embedding dimension of the regressor. Our objective is to obtain a minimum number of

false nearest neighbors for identifying a regressor with a minimal embedding dimension. More detailed procedures of the false nearest neighbors can be found in our earlier studies [26], [27]. In general, the percentage of false nearest neighbors decreases with an increasing embedding dimension and that may reach zero after the minimal embedding dimension is identified. Once the false nearest neighbors-based self-constructing strategy determines the system order (J), the architecture of the proposed SCWRNN can be then estimated. Next, the network parameters can be optimized by the following parameter optimization method.

C. RECURSIVE RECURRENT LEARNING ALGORITHM

In this paper, a recursive recurrent learning algorithm based on the concept of ordered derivatives is derived in parameter learning phase for improving the overall network performance [26]. In this paper, we combine the ordered derivative with a momentum term for each parameter update rules to accelerate the parameter learning convergence. In the learning phase, the optimization target is characterized to minimize the following error function with respect to the adjustable parameters ($\mathbf{w}$) of a network.

$$E(\mathbf{w}, k) = 1/2\,(y_d(k) - y(k))^2 = 1/2e(k)^2, \tag{9}$$

where $\mathbf{w}$ is the adjustable network parameters, $y_d(k)$ and $y(k)$ are the desired output and the actual output, respectively. The update rule for the network parameters is defined as follows:

$$\Delta w(k) = -\xi\left(\frac{\partial^+ E}{\partial w}\right) + \alpha \Delta w(k-1), \tag{10}$$

$$w(k) = w(k-1) + \Delta w(k), \tag{11}$$

where ξ is the learning rate and $\partial^+ E/\partial w$ is the ordered derivative which considers the direct and indirect effects on changing the parameter involved in the current state and previous states. $\alpha \Delta w$ is the momentum term, where $\alpha \in [0, 1]$ is the learning rate. The adjustable parameters $\mathbf{w}$ of the SCWRNN include the input link weights ($\mathbf{B} \in \mathbb{R}^{J\times P}$), the state matrix ($\mathbf{A} \in \mathbb{R}^{J\times J}$), and the output link weights ($\mathbf{C} \in \mathbb{R}^{m\times J}$). The current output $y(k)$ is obtained by calculating the activities of all nodes on each layer, and the corresponding functions are expressed as follows:

$$x_j(k) = \sum_{j=1}^{J}\left(\left(\sum_{i=1}^{J} a_{ji}x_i(k-1)\right) + \left(\sum_{h=1}^{P} b_{jh}u_h(k-1)\right)\right), \tag{12}$$

$$s = \mathbf{C}\mathbf{x}(k) = \sum_{j=1}^{J} c_j x_j(k), \tag{13}$$

$$y(k) = f(s) = \frac{\exp(s) - \exp(-s)}{\exp(s) + \exp(-s)}. \tag{14}$$

The update rule of the output link weights c_j is

$$c_j(k) = c_j(k-1) + \left(-\xi_{bc}\frac{\partial^+ E(k)}{\partial c_j} + \alpha \Delta c_j(k-1)\right), \tag{15}$$

$$\frac{\partial^+ E(k)}{\partial c_j} = \frac{\partial E(k)}{\partial c_j} = -e(k)x_j(k)\left(\frac{4}{(\exp(s) + \exp(-s))^2}\right), \tag{16}$$

where ξ_{bc} is the learning rate for adjusting c_j and b_{jh}.

To update the elements of the state matrix (a_{ji}) and the input link weights (b_{jh}), the current error signal should be propagated to not only the current state but also the previous states. The update rule of the components of the state matrix a_{ji} is

$$a_{ji}(k) = a_{ji}(k-1) + \left(-\xi_a\frac{\partial^+ E(k)}{\partial a_{ji}} + \alpha \Delta a_{ji}(k-1)\right), \tag{17}$$

$$\frac{\partial^+ E(k)}{\partial a_{ji}} = \frac{\partial E(k)}{\partial x_j(k)}\frac{\partial^+ x_j(k)}{\partial a_{ji}}, \tag{18}$$

$$\frac{\partial E(k)}{\partial x_j} = -c_j(k-1)\frac{4}{(\exp(s) + \exp(-s))^2}e(k), \tag{19}$$

$$\frac{\partial^+ x_j(k)}{\partial a_{ji}} = \frac{\partial x_j(k)}{\partial a_{ji}} + \frac{\partial x_j(k)}{\partial x_j(k-1)}\frac{\partial^+ x_j(k-1)}{\partial a_{ji}}, \tag{20}$$

where ξ_a is the learning rate for adjusting a_{jj}, $\partial x_j(k)/\partial a_{ji} = x_i(k-1)$, $\partial x_j(k)/\partial x_j(k-1) = a_{jj}(k-1)$, and $\partial x_j(1)/\partial a_{ji} = x_i(0)$ when $k = 1$.

The update rule of the input link weights b_{jh} is:

$$b_{jh}(k) = b_{jh}(k-1) + \left(-\xi_{bc}\frac{\partial^+ E(k)}{\partial b_{jh}} + \alpha \Delta b_{jh}(k-1)\right), \tag{21}$$

$$\frac{\partial^+ E(k)}{\partial b_{jh}} = \frac{\partial E(k)}{\partial x_j(k)}\frac{\partial^+ x_j(k)}{\partial b_{jh}}, \tag{22}$$

where $\partial x_j(k)/\partial b_{jh} = u_h(k-1)$ and $\partial^+ x_j(1)/\partial b_{jh} = u_h(0)$ when $k = 1$. The values of $\partial^+ x_j(k)/\partial a_{ji}$and $\partial^+ x_j(k)/\partial b_{jh}$are set to zero initially and recursively accumulated as the error signal generated by each training measurement. In addition, to avoid a large accumulated error, the values of these terms are reset to zero after a period of learning. More detailed information of the recursive recurrent learning algorithm for the SCWRNN can be found in our earlier study [26].

III. RANDOM DRIFT MODELING AND COMPENSATION ALGORITHM

This paper focuses on the development of a random drift modeling and compensation algorithm which is based on the SCWRNN to model the random drift of the MEMS-based gyroscopes for improving the accuracy of estimated orientations and reconstructed trajectories. Once the calibrated angular velocity signals are obtained from the calibration process, which can eliminate the scale factor errors and biases (deterministic errors) of the MEMS-based gyroscopes, a SCWRNN is then applied to model the random drift (stochastic errors) of the gyroscopes. From our literature review, the gyroscope error is the primary bottleneck for enhancing the performance of the estimated motion orientations and reconstructed trajectories [15]. An uncompensated gyroscope error introduces a first-order error in orientation angles after single integral.

Therefore, when the acceleration is transferred from the body coordinate (body frame) to the reference coordinate (local-level frame), the acceleration vector will be incorrectly transferred due to the orientation estimation error. Subsequently, the error of acceleration in the reference coordinate will lead to a first-order and a second-order error in the velocity and position (trajectory) after single integral and double integral, respectively. Hence, the position (trajectory) error caused by the gyroscope error grows very rapidly with time (a third-order error in the position).

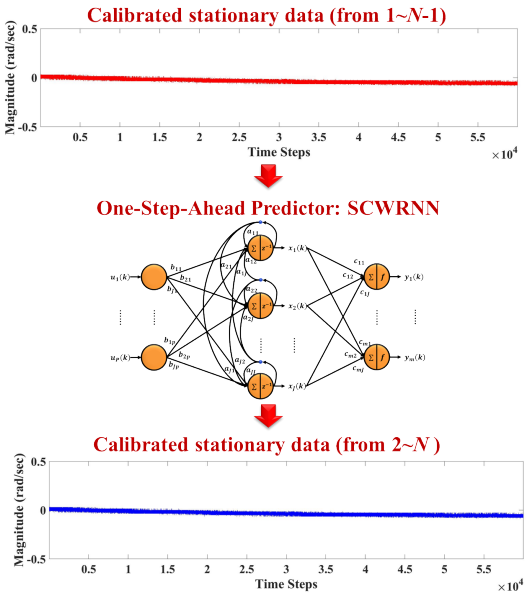

FIGURE 2. The procedure of the one-step-ahead predictor for modeling the random drift of the MEMS-gyroscopes through the proposed SCWRNN.

The proposed SCWRNN is applied to model the random drift by using the time series measurements of the MEMS-gyroscopes, where that is stationary. In this study, the proposed SCWRNN is trained as a one-step-ahead predictor in the modeling procedure using the stationary measurements of the MEMS-based gyroscope. That is, the gyroscope readings of the stationary measurement from 1 to N-1 and from 2 to N are represented as the input and output data for the proposed SCWRNN, respectively, where N is the length of the measurement [28]. The one-step-ahead predictor procedure for modeling the random drift of the MEMS-gyroscopes is shown in Fig. 2. In general, the measured angular velocity signal generated from the handwriting motion is always accompany with the random drift signal which can be modeled by the calibrated stationary angular velocity signal of the MEMS-based gyroscope. Hence, the calibrated stationary angular velocity signal should be the input for the one-step-ahead predictor (SCWRNN) for modeling the random drift signal. After then, each collected handwriting angular velocity signal is utilized to subtract the estimated random drift signal for obtaining the drift-removal handwriting angular velocity, which can be used to estimate accurate handwriting orientation angles and reconstructed trajectories. The procedure of the random drift modeling and compensation algorithm is shown as Fig. 3.

IV. EXPERIMENTAL SETUP AND RESULTS

A. EXPERIMENTAL SETUP

In this paper, the pen-type inertial-sensing-based HCI device (IMUPEN) implemented in our earlier work [13] is composed of a microcontroller (C8051F206 with 12 bits A/D converter), an RF wireless transmission module (nRF2401), a triaxial accelerometer (LIS3L02AQ3), a biaxial angular rate gyroscope (IDG-300), a uniaxial angular rate gyroscope (ADXRS300), and a power supply circuit. The size of the IMUPEN is 125 mm $\times$ 15 mm $\times$ 15 mm as shown in Fig. 4. The microcontroller is utilized to collect the analog acceleration and angular velocity signals, to convert the signals to digital ones via an internal 12 bits A/D converter, and to transmit the signals to a PC via the RF wireless transceiver. The accelerometer can detect the gravitational and X-, Y-, and Z-axis handwriting motion accelerations of the IMUPEN held by users during handwriting activities, and has a full scale of $\pm$2g in this paper. The IDG-300 gyroscope can simultaneously sense the X- and Y-axis handwriting angular velocities of the IMUPEN, and its full-scale range and sensitivity are set as $\pm$500 °/s and 2.0 mV/°/s, respectively. The ADXRS300 gyroscope measures the Z-axis handwriting angular velocity of the IMUPEN, and its full-scale range and sensitivity are set as $\pm$300 °/s and 5.0 mV/°/s, respectively. The sampling rate of the accelerometer and gyroscopes were set as 100 Hz. The power supply circuit is used to provide the power consumption for the IMUPEN, which is composed of a Li-ion battery, a Li-ion battery charging module, and regulators. The overall power consumption of the IMUPEN is 30 mA at 3.7 V.

B. RANDOM DRIFT MODELING AND COMPENSATION OF MEMS-BASED GYROSCOPE

In this paper, we collected the stationary angular velocity measurements contaminated by the random drift of the MEMS-based gyroscopes for modeling the random drift and compensating them from the calibrated angular velocities. In the following presentation, we utilize the calibrated X-axis angular velocity (ω_{cx}) measured by the MEMS-based gyroscope to interpret the conception of the proposed SCWRNN for the random drift removal. We collected two different stationary angular velocity measurements of the MEMS-based gyroscope for 10 minutes, whose output signal was sampled at 100 Hz. Hence, each stationary angular velocity measurement contaminated by the random drift consists of 60,000 data and the unit is in radians per second (rad/sec). The first stationary angular velocity measurement was used to be the training data for the proposed SCWRNN to model the gyroscope random drift, while the second stationary angular velocity measurement was treated as the testing data for verifying the modeling performance of the proposed SCWRNN. Note that the calibration procedure is utilized to eliminate

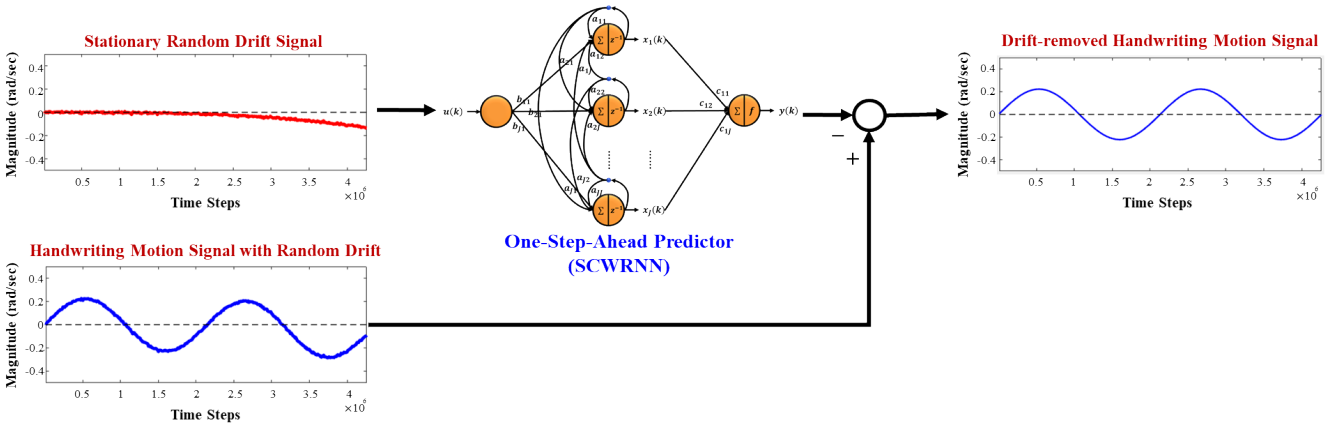

FIGURE 3. The proposed random drift modeling and compensation process through the proposed SCWRNN.

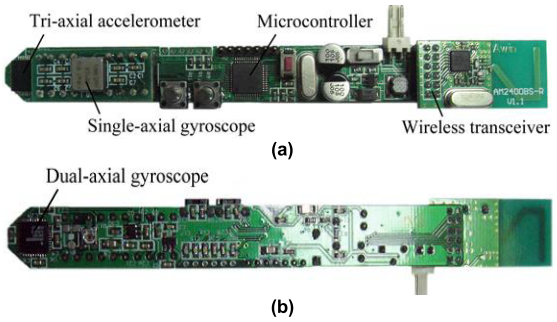

FIGURE 4. The proposed IMUPEN. (a) Front view of the hardware circuit. (b) Back view of the hardware circuit.

the deterministic errors (scale factor error and bias) of the all stationary angular velocity measurements. More information about the calibration procedure of the gyroscopes can be found in [13].

The random drift modeling and compensation procedure of the stationary gyroscope measurement is shown Fig. 3. In the modeling procedure, we utilized the first stationary angular velocity measurement to train the proposed SCWRNN to be as a one-step-ahead predictor. That is, from 1 to 59,999 and from 2 to 60,000 of the first stationary angular velocity measurement were treated as the input and output data for the proposed SCWRNN, respectively. The learning rates ξ_a and ξ_{bc} were set as 0.05 and 0.5, respectively. In the beginning, the false nearest neighbors utilized the first 500 stationary angular velocity measurement to determine the system order (number of state variables or hidden neurons) of the whole SCWRNN. From Table 1, the system order of the SCWRNN applied to model the gyroscope random drift is chosen as 6. The total number of the network parameters is 48. Subsequently, the remaining stationary angular velocity measurements are used to optimize the network parameters by the recursive recurrent learning algorithm. The state-space equations of trained network are represented in (23), as shown at the bottom of the next page, where $\mathbf{x}(k) = [x_1(k), x_2(k), x_3(k), x_4(k), x_5(k), x_6(k)]^T$ are the state variables.

TABLE 1. Embedding dimensions vs. percentages of false nearest neighbors ($P_{\mathbf{fnn}}$) for modeling the X-axis gyroscope random drift.

J	l	P_{fnn} (%)
0	0	100.0
1	0	93.5
1	1	76.8
2	1	59.0
2	2	52.0
3	2	36.8
3	3	24.8
4	3	14.2
4	4	6.4
5	4	3.4
5	5	1.2
6	5	0.0

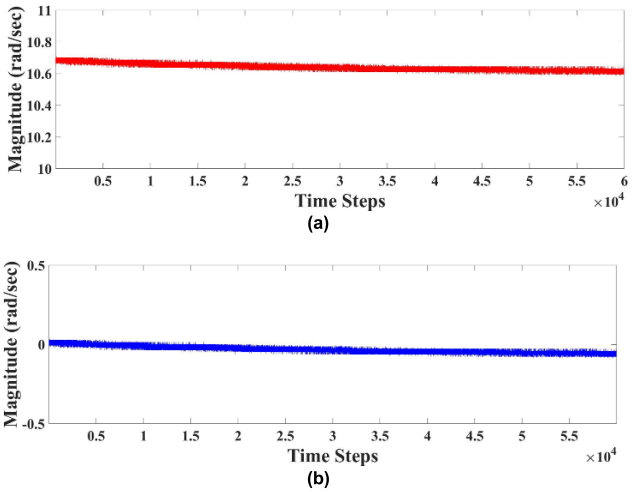

FIGURE 5. Gyroscope reading of the second stationary data. (a) Raw data. (b) Calibrated data.

After the network was trained, the second stationary angular velocity measurement of the gyroscope was utilized to evaluate the ability and suitability of the proposed SCWRNN to generalize for a different measurement. Fig. 5 shows the second stationary angular velocity measurement

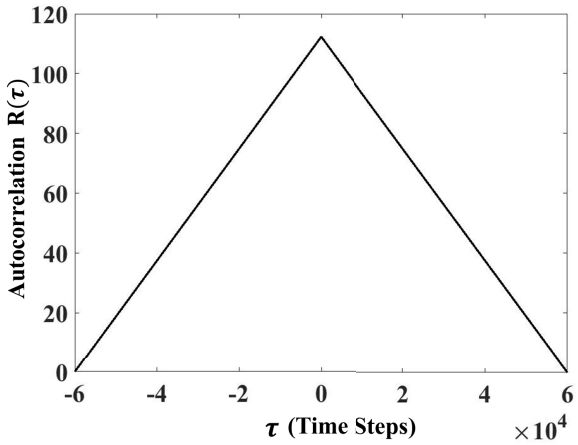

FIGURE 6. Autocorrelation of the second stationary raw angular velocity.

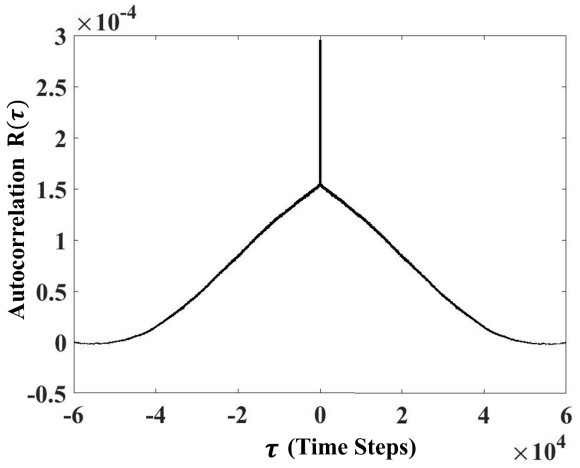

FIGURE 7. Autocorrelation of the second stationary angular velocity after removing the scale factor error and bias.

contaminated by the random drift before and after the calibration procedure. The raw stationary data collected from the gyroscope is shown in Fig. 5(a). The stationary signal shown in Fig. 5(b) was calibrated via the calibration procedure to remove the scale factor error and bias. Fig. 6 gives the autocorrelation of the stationary raw angular velocity measured by the gyroscope. Fig. 7 shows the autocorrelation of the stationary gyroscope measurement after removing the scale factor error and bias. Fig. 8 presents the stationary angular velocity measurement (after removing the scale factor error and bias) from 2 to 60,000 together with the estimated random drift by the proposed SCWRNN that used the readings from 1 to 59,999 as the inputs. In addition, we applied the mean square error (MSE), mean absolute error (MAE), root mean square error (RMSE), and average relative error (ARE) to evaluate the estimation performance, which are briefly described as follows:

$$MSE = \frac{1}{n}\sum_{i=1}^{n}(\omega_i - \widehat{\omega}_i)^2, \tag{24}$$

$$MAE = \frac{1}{n}\sum_{i=1}^{n}|\omega_i - \widehat{\omega}_i|, \tag{25}$$

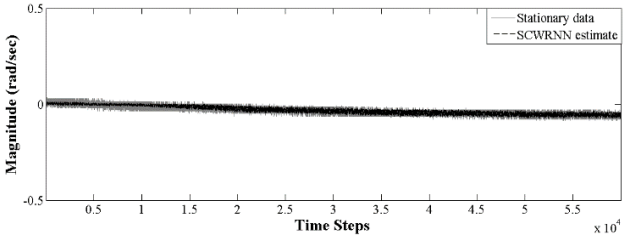

FIGURE 8. The stationary angular velocity after removing the scale factor error and bias (gray color) versus the SCWRNN prediction of the random drift (black color).

$$RMSE = \sqrt{\frac{\sum_{i=1}^{n}(\omega_i - \widehat{\omega}_i)^2}{n}}, \tag{26}$$

$$ARE = \frac{1}{n}\sum_{i=1}^{n}\frac{|\omega_i - \widehat{\omega}_i|}{\omega_i}, \tag{27}$$

where n is the size of the stationary angular velocity measurement, ω_i represents the actual stationary angular velocity measurement, and $\widehat{\omega}_i$ denotes the predicting stationary angular velocity measurement. The MSE, MAE, RMSE, and

$$\mathbf{x}(k+1) = \begin{bmatrix} -0.2505 & -0.4135 & -0.1993 & 0.1246 & -0.3985 & -0.4519 \\ -0.4524 & -0.1867 & -0.4007 & -0.4044 & 0.3323 & 0.1686 \\ -0.0546 & -0.0477 & -0.2003 & -0.4227 & -0.1656 & 0.1030 \\ -0.4906 & -0.3954 & -0.4554 & 0.2803 & -0.2020 & 0.0274 \\ 0.3899 & 0.5014 & 0.0028 & 0.4115 & 0.2531 & 0.2329 \\ -0.3248 & -0.1512 & 0.2556 & 0.0530 & -0.4723 & 0.2202 \end{bmatrix} \mathbf{x}(k) + \begin{bmatrix} 0.1304 \\ -0.2298 \\ -0.3445 \\ -0.2961 \\ 0.3626 \\ -0.5591 \end{bmatrix} u(k),$$

$$y(k) = \mathbf{F}([0.5372 \; -0.4412 \; 0.2744 \; -0.1846 \; -0.3266 \; -0.5423]\,\mathbf{x}(k)), \tag{23}$$

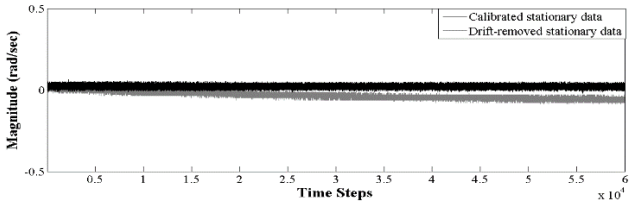

FIGURE 9. Gyroscope reading of the second stationary signal. (Gray color: without removing drift signal; black color: random drift-removed signal.)

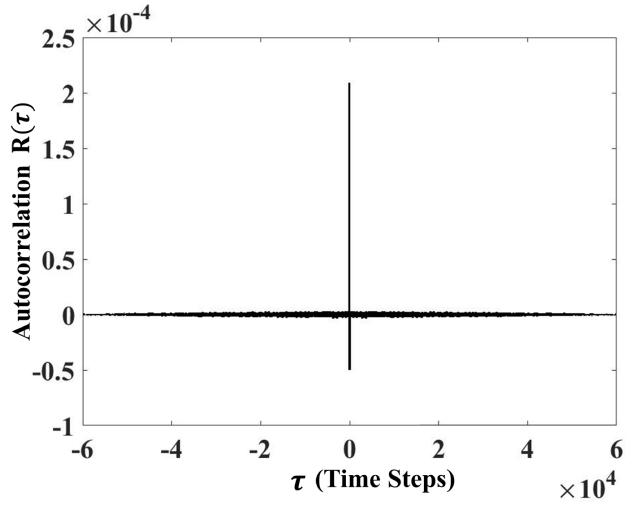

FIGURE 10. Autocorrelation of the second stationary angular velocity after removing the scale factor error, bias, and random drift estimated by the SCWRNN.

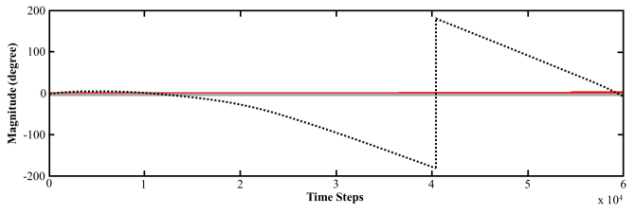

FIGURE 11. Orientation angle obtained through the integral of the stationary angular velocity measurements. (Gray solid curve: ideal orientation angle, red solid curve: orientation angle estimation with removing drift signal, black dotted curve: orientation angle estimation without removing drift signal).

ARE were 0.0018 rad/sec, 0.0358 rad/sec, 0.042 rad/sec, and 3.4336 %, respectively. The results show that the proposed SCWRNN can model the random drift of the MEMS-based gyroscope effectively. Fig. 9 shows the stationary signal after removing the scale factor error, bias, and estimated random drift. Fig. 10 shows the autocorrelation of the stationary gyroscope signal after eliminating the scale factor error, bias, and random drift estimated by the proposed SCWRNN. Obviously, the stationary angular velocity measurement after removing the scale factor error, bias, and estimated random drift mainly contained white noise. Fig. 11 shows the orientation angles caused by the integral of the random drift of the gyroscope and by the integral of the random drift removal signal, respectively. Obviously, the ideal orientation angle should be zero when the gyroscope embedded in the IMUPEN was stationary. We can see that if the random drift was not removed, the error of the orientation angle estimation continuously increased. The error of the orientation angle arrived about 360° in 10 minutes. In contrast, the estimated orientation angle was very close to zero if the random drift was removed by the proposed random drift modeling and compensation algorithm. Finally, the drift-removal measurements of gyroscopes can be obtained by removing the random drift estimated by the SCWRNN from the calibrated gyroscope measurements.

C. HANDWRITTNG TRAJECTORY RECONSTRUCTION APPLICATIONS

After modeling and compensation of the random drift of the gyroscopes, we utilized the handwriting trajectory reconstruction algorithm to reconstruct handwriting trajectories by using the calibrated accelerations and compensated angular velocities. The handwriting trajectory reconstruction algorithm consists of the following procedures: 1) signal acquisition, 2) calibration, 3) random drift modeling and compensation, 4) lowpass filtering, 5) orientation estimation, 6) coordinate transformation and gravity compensation, and 7) handwriting trajectory reconstruction. At the beginning of the procedures, the handwriting motion signals measured from the accelerometer and gyroscopes were collected by the microcontroller embedded in the IMUPEN and then transmitted to the PC via the RF wireless transmission module. Second, a calibration process was utilized to eliminate the deterministic errors (scale factor errors and biases) of the accelerometer and gyroscopes. Third, the proposed random drift modeling and compensation algorithm was developed for removing the stochastic errors (random drift) of the gyroscopes. Fourth, a digital lowpass filter was designed for removing high frequency noise of the inertial signals and users' unconscious trembles. Fifth, a quaternion-based orientation estimation method was used to estimate accurate orientation angles of the IMUPEN for forming a transformation matrix. Sixth, the coordinate transformation and gravity compensation procedure was utilized to transfer the filtered acceleration from the body coordinate to the reference coordinate and to eliminate the effect of the gravitational acceleration in the reference coordinate. Finally, the handwriting trajectory of the IMUPEN was reconstructed via the multi-axis dynamic (MAD) switch. The block diagram of the proposed handwriting trajectory reconstruction algorithm is shown in Fig. 12. More detailed information for the handwriting trajectory reconstruction procedures can be found in [13].

In this experiment, participants were asked to write digits using the IMUPEN without ambit restrictions. Fig. 13 shows the experimental setup. All the participants were asked to complete each digit in one stroke and follow the pictorial trajectories of the digits shown as Fig. 14(a). Before the experiment, we asked all the participants to practice writing of the

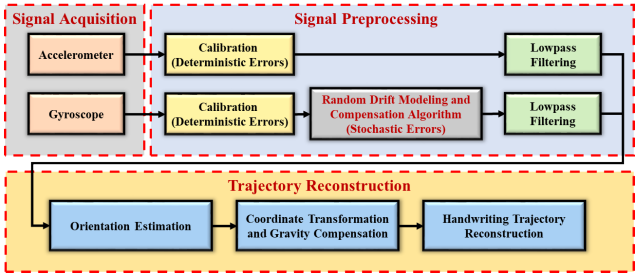

FIGURE 12. Handwriting trajectory reconstruction algorithm with the proposed random drift modeling and compensation algorithm.

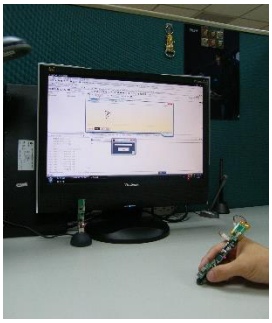

FIGURE 13. The handwritten digit recognition experimental settings.

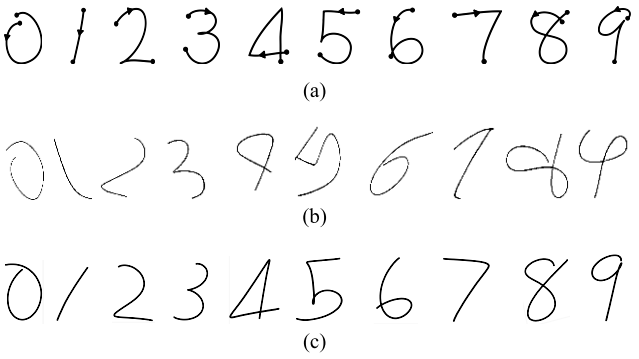

FIGURE 14. The trajectories of the 10 digits. (a) The pictorial digit trajectories. (b) The digit trajectories using the IMUPEN and its associated handwriting trajectory reconstruction algorithm without the random drift modeling and compensation algorithm. (c) The digit trajectories using the IMUPEN and its associated handwriting trajectory reconstruction algorithm with the gyroscope drift removal through the random drift modeling and compensation algorithm.

digits using the IMUPEN until they felt comfortable. The proposed handwriting trajectory reconstruction algorithm was utilized to reconstruct the trajectories based on the accelerations and angular velocities generated by the IMUPEN during handwriting motions. The digit trajectories collected from a participant using the IMUPEN and its associated handwriting trajectory reconstruction algorithm without/with gyroscope drift removal through the proposed random drift modeling and compensation algorithm are shown in Figs. 14(b) and (c), respectively. Obviously, from Fig. 14(b), we can see that if the random drift of the gyroscope was not removed, the handwriting trajectories were crooked or distorted due to the error of the orientation angle estimation. However, from Fig. 14(c), if the random drift is removed through the proposed random drift modeling and compensation algorithm, the handwriting trajectories can easily be recognized by human beings due to the correct orientation angle estimation.

V. CONCLUSIONS

In this paper, we present a random drift modeling and compensation algorithm to model and compensate the random drift of the MEMS-based gyroscopes, which is composed of the SCWRNN with the false nearest neighbors-based self-constructing strategy for determining network structure and the recursive recurrent learning algorithm for optimizing network parameters. For modeling the random drift, the MSE, MAE, RMSE, and ARE of the modeling error are 0.0018 rad/sec, 0.0358 rad/sec, 0.042 rad/sec, and 3.4336 %, respectively. The results show that the proposed SCWRNN can model the gyroscope random drift effectively. And then, the proposed random drift modeling and compensation algorithm is integrated into the handwriting trajectory reconstruction algorithm of the IMUPEN for handwriting trajectory reconstruction applications. The experimental results show that the digit trajectories collected from the participants using the IMUPEN and its associated handwriting trajectory reconstruction algorithm without gyroscope drift removal were crooked or distorted due to the error of the orientation angle estimation. In contrast, the digit trajectories can easily be recognized by human beings if the random drift is removed through the proposed random drift modeling and compensation algorithm. Based on the abovementioned experimental results, the effectiveness of the proposed SCWRNN-based random drift modeling and compensation scheme for the MEMS-based gyroscopes has been successfully validated and applied in the handwriting trajectory reconstruction applications.

REFERENCES

[1] H.-C. Chang, Y.-L. Hsu, S.-C. Yang, J.-C. Lin, and Z.-H. Wu, "A wearable inertial measurement system with complementary filter for gait analysis of patients with stroke or Parkinson's disease," *IEEE Access*, vol. 4, pp. 8442–8453, 2017.

[2] G. Du, P. Zhang, and D. Li, "Human–manipulator interface based on multisensory process via Kalman filters," *IEEE Trans. Ind. Electron.*, vol. 61, no. 10, pp. 5411–5418, Oct. 2014.

[3] B. Fang, F. Sun, H. Liu, D. Guo, W. Chen, and G. Yao, "Robotic teleoperation systems using a wearable multimodal fusion device," *Int. J. Adv. Robotic Syst.*, vol. 14, no. 4, pp. 1–11, 2017.

[4] M. Kos and I. Kramberger, "A wearable device and system for movement and biometric data acquisition for sports applications," *IEEE Access*, vol. 5, pp. 6411–6420, 2017.

[5] Y.-L. Hsu, S.-C. Yang, H.-C. Chang, and H.-C. Lai, "Human daily and sport activity recognition using a wearable inertial sensor network," *IEEE Access*, vol. 6, pp. 31715–31728, 2018.

[6] H. Huang *et al.*, "Attitude estimation fusing Quasi-Newton and cubature Kalman filtering for inertial navigation system aided with magnetic sensors," *IEEE Access*, vol. 6, pp. 28755–28767, 2018.

[7] G. Sprint, D. J. Cook, D. L. Weeks, and V. Borisov, "Predicting functional independence measure scores during rehabilitation with wearable inertial sensors," *IEEE Access*, vol. 3, pp. 1350–1366, 2015.

[8] X. Wu, R. Shen, L. Fu, X. Tian, P. Liu, and X. Wang, "iBILL: Using iBeacon and inertial sensors for accurate indoor localization in large open areas," *IEEE Access*, vol. 5, pp. 14589–14599, 2017.

[9] Y. Wang, Y. Zhao, R. H. M. Chan, and W. J. Li, "Volleyball skill assessment using a single wearable micro inertial measurement unit at wrist," *IEEE Access*, vol. 6, pp. 13758–13765, 2018.
[10] E. Villeneuve, W. Harwin, W. Holderbaum, B. Janko, and R. S. Sherratt, "Reconstruction of angular kinematics from wrist-worn inertial sensor data for smart home healthcare," *IEEE Access*, vol. 5, pp. 2351–2363, 2017.
[11] K. Altun, B. Barshan, and O. Tunçel, "Comparative study on classifying human activities with miniature inertial and magnetic sensors," *Pattern Recognit.*, vol. 43, no. 10, pp. 3605–3620, Oct. 2010.
[12] N. Dawar and N. Kehtarnavaz, "Real-time continuous detection and recognition of subject-specific smart tv gestures via fusion of depth and inertial sensing," *IEEE Access*, vol. 6, pp. 7019–7028, 2018.
[13] J.-S. Wang, Y.-L. Hsu, and J.-N. Liu, "An inertial-measurement-unit-based pen with a trajectory reconstruction algorithm and its applications," *IEEE Trans. Ind. Electron.*, vol. 57, no. 10, pp. 3508–3521, Oct. 2010.
[14] D. Vlasic *et al.*, "Practical motion capture in everyday surroundings," *ACM Trans. Graph.*, vol. 26, no. 3, 2007, Art. no. 35.
[15] J. Georgy, A. Noureldin, M. J. Korenberg, and M. M. Bayoumi, "Modeling the stochastic drift of a MEMS-based gyroscope in gyro/odometer/GPS integrated navigation," *IEEE Trans. Intell. Transp. Syst.*, vol. 11, no. 4, pp. 856–872, Dec. 2010.
[16] D. Bhatt, P. Aggarwal, P. Bhattacharya, and V. Devabhaktuni, "An enhanced MEMS error modeling approach based on nu-support vector regression," *Sensors*, vol. 12, no. 7, pp. 9448–9466, 2012.
[17] M. Tamazin, A. Noureldin, and M. J. Korenberg, "Robust modeling of low-cost MEMS sensor errors in mobile devices using fast orthogonal search," *J. Sensors*, vol. 2013, May 2013, Art. no. 101820.
[18] A. Noureldin, T. B. Karamat, M. D. Eberts, and A. El-Shafie, "Performance enhancement of MEMS-based INS/GPS integration for low-cost navigation applications," *IEEE Trans. Veh. Technol.*, vol. 58, no. 3, pp. 1077–1096, Mar. 2009.
[19] Y. Zhang and J. Fang, "Research on the random error modeling and compensation method for MEMS gyro," in *Proc. SPIE 6th Int. Symp. Instrum. Control Technol., Sensors, Autom. Meas., Control, Comput. Simul.*, vol. 6358, Oct. 2006, pp. 63580G-1–63580G-5.
[20] W. Hao and W. Tian, "Modeling the random drift of micro-machined gyroscope with neural network," *Neural Process. Lett.*, vol. 22, no. 3, pp. 235–247, 2005.
[21] R. Sharaf and A. Noureldin, "A neural network model of optical gyros drift errors with application to vehicular navigation," in *Proc. SPIE Appl. Digit. Image Process. XXVII*, vol. 5558, Aug. 2004, pp. 13–20.
[22] H. Xing, B. Hou, Z. Lin, and M. Guo, "Modeling and compensation of random drift of MEMS gyroscopes based on least squares support vector machine optimized by chaotic particle swarm optimization," *Sensors*, vol. 17, no. 10, p. 2335, 2017.
[23] S. Chong *et al.*, "Temperature drift modeling of MEMS gyroscope based on genetic-Elman neural network," *Mech. Syst. Signal Process.*, vols. 72–73, pp. 897–905, May 2016.
[24] H. D. I. Abarbanel and M. B. Kennel, "Local false nearest neighbors and dynamical dimensions from observed chaotic data," *Phys. Rev. E, Stat. Phys. Plasmas Fluids Relat. Interdiscip. Top.*, vol. 47, no. 5, pp. 3057–3068, 1993.
[25] J. M. Nichols and J. D. Nichols, "Attractor reconstruction for non-linear systems: A methodological note," *Math. Biosci.*, vol. 171, no. 1, pp. 21–32, 2001.
[26] Y.-L. Hsu and J.-S. Wang, "A Wiener-type recurrent neural network and its control strategy for nonlinear dynamic applications," *J. Process Control*, vol. 19, no. 6, pp. 942–953, 2009.
[27] J.-S. Wang, Y.-L. Hsu, H.-Y. Lin, and Y.-P. Chen, "Minimal model dimension/order determination algorithms for recurrent neural networks," *Pattern Recognit. Lett.*, vol. 30, no. 9, pp. 812–819, 2009.
[28] Y.-L. Hsu, P.-H. Chou, and Y.-C. Kuo, "Drift modeling and compensation for MEMS-based gyroscope using a wiener-type recurrent neural network," in *Proc. 4th IEEE Int. Symp. Inertial Sensors Syst.*, Mar. 2017, pp. 39–42.

YU-LIANG HSU (M'17) received the B.S. degree in automatic control engineering from Feng Chia University, Taichung, Taiwan, in 2004, and the M.S. and Ph.D. degrees in electrical engineering from National Cheng Kung University, Tainan, Taiwan, in 2007 and 2011, respectively.

He is currently an Associate Professor with the Department of Automatic Control Engineering, Feng Chia University. His research interests include computational intelligence, biomedical engineering, nonlinear system identification, and wearable intelligent technology.

JEEN-SHING WANG (S'94–M'02) received the B.S. and M.S. degrees in electrical engineering from the University of Missouri, Columbia, in 1996 and 1997, respectively, and the Ph.D. degree from Purdue University, West Lafayette, IN, USA, in 2001.

He is currently a Distinguished Professor with the Department of Electrical Engineering, National Cheng Kung University, Taiwan. His research interests include computational intelligence, design of wearables, big data analysis, and system optimization.